ACS OMEGA

Open Access
This article is licensed under CC-BY-NC-ND 4.0

http://pubs.acs.org/journal/acsodf
Article

$Ti_3C_2T_x$ MXene Additives for Enhanced Pool Boiling Regime

Saketh Merugu, Md Moynul Hasan, Anupma Thakur, Jacob Patenaude, Babak Anasori, George Choueiri, and Anju Gupta*

Cite This: *ACS Omega* 2025, 10, 6534−6543

Read Online

ACCESS | Metrics & More | Article Recommendations | Supporting Information

ABSTRACT: This study investigates the potential applications of MXenes as an additive in heat-exchanging fluids under atmospheric pressure conditions. A low concentration of 0.1 wt % titanium carbide ($Ti_3C_2T_x$) MXene-enhanced deionized water altered the boiling regime by demonstrating high critical heat flux (CHF) of 2110.1 kW/m^2 and heat transfer coefficient (HTC) 163.6 kW/m^2 °C, representing a 70.1% increase in CHF and a 213.5% increase in HTC compared to deionized water. Rheological studies were conducted to determine the optimal MXene concentration for long-term stability in the base fluid, ensuring suitability for large-scale industrial applications. Notably, $Ti_3C_2T_x$ MXene dispersion demonstrated an 11% enhancement in CHF and a 45% enhancement in HTC compared to the highest reported values for Ag/ZnO-enhanced fluids on plain copper substrates in the literature. This shift in boiling regime is attributed to a combined mechanisms involving thermophoretic and Brownian motion that facilitated the circulation of the $Ti_3C_2T_x$ MXene flakes before their stratification on the copper heater surface, which further led to improved interfacial properties such as surface roughness, wettability, and conductivity. This study provides insights on rheological property modulation and $Ti_3C_2T_x$ MXene enhanced heat transfer fluid-surface interactions in pool boiling efficiency.

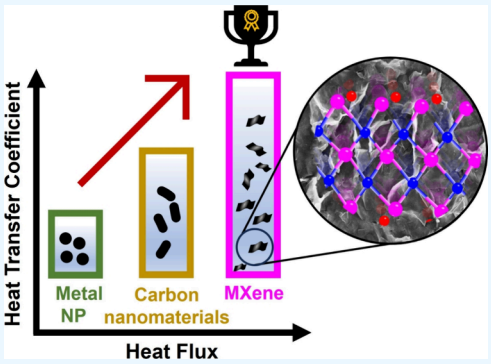

1. INTRODUCTION

Nanoparticle additives in heat-exchanging fluids also known as nanofluids, have revolutionized thermal management, consistently demonstrating major enhancements in thermal conductivity and heat transfer coefficients.[1] Among these nanoparticle additives, metal nanoparticles such as copper, aluminum, silver, and their oxides have demonstrated remarkable improvements in overall thermal performance.[2,3] These enhancements are especially pronounced in boiling heat transfer, a highly effective method of heat dissipation extensively used in power generation, electronics cooling, and thermal management systems.[4−6] The effectiveness of nanoparticles in enhancing boiling heat transfer is attributed to multiple mechanisms, including increased thermal conductivity, Brownian motion, nanolayer formation at liquid-particle interfaces, and clustering effects.[7] Additionally, nanoscale additives offer significant advantages, achieving substantial thermal improvements at lower concentrations compared to larger particles, particularly at higher Reynolds numbers.[8] Their ability to improve the thermal conductivity of bulk boiling fluid even at low concentrations makes them particularly efficient for boiling heat transfer which is characterized by high critical heat flux (CHF) and heat transfer coefficient (HTC).[9]

Despite their remarkable thermal performance, the applications of metal nanoparticles are limited by their susceptibility to oxidation and concerns regarding long-term stability, particularly when compared to their more robust ceramic or metal oxide counterparts.[10,11] These limitations have led researchers to explore various oxide-based nanofluids, including TiO_2,[12] Al_2O_3,[13] CuO,[14] Fe_3O_4,[15] ZnO,[16] and SiO_2,[17] which have been explored and have reported high HTC and CHF. Concurrently, with the emergence of advanced 2D materials such as carbon-nanomaterials, borophene, and metal−organic frameworks (MOFs) have pioneered advances in energy harvesting, storage, and electronics.[1−3] Additionally, as additives and coatings, these contemporary 2D materials significantly enhance performance and functionality across various industries often surpassing the capabilities of traditional nanofluids. Our previous work on GNPs based coating also yielded record-breaking critical heat flux of (CHF) of 289 W/cm^2 achieved at the lowest recorded wall superheat temperature of 2.2 °C for flat surfaces.[18,19] GNPs have also demonstrated remarkable improvements in thermal conductivity and heat transfer coefficients when used in nanofluids. GNP-based aqueous nanofluids have shown thermal conductivity enhancements of up to 25% at low concentrations.[20] The specific mechanisms contributing to the improved boiling performance are attributed to nanoparticle deposition,

Received: July 30, 2024
Revised: January 23, 2025
Accepted: January 31, 2025
Published: February 5, 2025

Downloaded via 72.240.198.73 on June 24, 2025 at 21:50:34 (UTC).
See https://pubs.acs.org/sharingguidelines for options on how to legitimately share published articles.

ACS Publications
© 2025 The Authors. Published by American Chemical Society

https://doi.org/10.1021/acsomega.4c06988
ACS Omega 2025, 10, 6534−6543

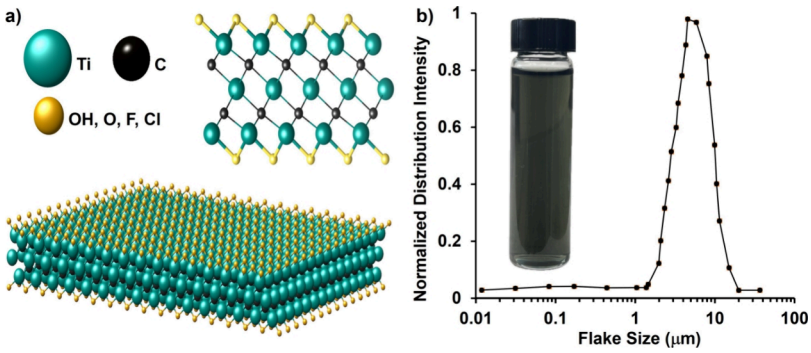

Figure 1. (a) Schematic representation of $Ti_3C_2T_x$ *MXene, (b) flake size distribution of* $Ti_3C_2T_x$ *MXene dispersion in deionized (DI) water along with photographic image.*

alteration of bubble dynamics, enhancement of thermal conductivity, and improved liquid supply to the evaporating thin film.[21−23] Specifically, by delaying the onset of critical heat flux to higher values of wall heat flux via deposition of nanoparticles on the heating surface,[24] that improves surface wettability and capillary action.[20,25] This expansion of the effective nucleate boiling region allows for more efficient heat dissipation across a broader range of operating conditions. While traditional and contemporary materials offer great potential, their successful application in heat transfer systems necessitates a nuanced approach.[26] Key considerations include optimizing particle concentration, ensuring long-term suspension stability, and controlling potential deposition on heat transfer surfaces.[27,28] When these factors are carefully balanced, the resulting formulations can yield transformative benefits: enhanced system efficiency, reduced maintenance requirements, and extended equipment lifespan. These advantages position well-designed nanofluids as indispensable components in modern thermal management solutions.[29−31]

MXenes, a family of two-dimensional (2D) transition metal carbides, nitrides, and carbonitrides, were first discovered in 2011.[32] Among this innovative class of materials, titanium carbide ($Ti_3C_2T_x$) MXene combines the inherent advantages of titanium-based materials with the unique properties afforded by its 2D nanostructure. The synergy of these characteristics, positions $Ti_3C_2T_x$ MXene as a promising candidate for advancing thermal management solutions. One of the key attributes of $Ti_3C_2T_x$ MXene is its high thermal conductivity, measured at approximately 55.8 W/m °C[33] that may enable efficient heat dissipation from the heating surface to the bulk fluid, which can enhance boiling heat transfer. The unique 2D structure of MXene flakes is hypothesized to offer dual benefits in heat transfer applications. First, it is expected to enhance surface wetting on the heater surface. Second, it may create a porous layer that could promote bubble nucleation and delay the onset of film boiling. Furthermore, their large surface area and excellent colloidal stability, evidenced by zeta potential values typically ranging from −40 to −60 mV when measured in water,[34] ensures uniform dispersion and long-term performance in liquid environments such as in boiling heat transfer applications, which is unexplored.

This study aims to address this research gap and expand the current understanding of MXenes in thermal applications by investigating the performance of $Ti_3C_2T_x$ MXene dispersions in pool boiling heat transfer. Our comprehensive investigation involved studying pool boiling heat transfer characteristics of $Ti_3C_2T_x$ MXene dispersions informed by rheology yielded high CHF and HTC compared to the dispersions reported in the literature of plain and textured surfaces. The unique thermal properties and nonspherical shape of $Ti_3C_2T_x$ MXene flakes contribute to these impressive performance metrics. In this study, the deposition of $Ti_3C_2T_x$ MXene 2D flakes resulted in changes in surface wettability. We propose that a combination of thermophoretic-led Brownian motion and stratification phenomena are key contributors to the observed high CHF and HTC values. This hypothesis provides new insights into the mechanisms underlying the enhanced heat transfer performance of MXene dispersions. The novelty of this study lies in its focused exploration of $Ti_3C_2T_x$ MXene, a flagship material in the MXene family, within the context of thermal engineering. By bridging the gap between advanced materials science and practical thermal management applications, this research opens new avenues for developing highly efficient cooling solutions using contemporary 2D materials.

2. MATERIALS AND METHODS

2.1. Preparation and Rheology of $Ti_3C_2T_x$ MXene Dispersions. $Ti_3C_2T_x$ MXene was synthesized by wet-chemical selective etching of Ti_3AlC_2 MAX illustrated in Figure 1a. The specific procedures for etching, intercalation, and annealing are detailed in a prior study.[34] 1 g of Ti_3AlC_2 MAX was rinsed in 9 M HCl for 18 h to remove intermetallic impurities. The washed material was then etched in a mixture of 12 M HCl, deionized water, and 28.4 M HF (6:3:1 by volume) for 24 h at 35 °C, stirring at 400 rpm. The etched MXene was further rinsed with deionized water via centrifugation until pH ∼6. For delamination, the MXene sediment was added to LiCl solution, stirred for 1 h at 65 °C under argon flow, and then rinsed again. Finally, the mixture was vortexed for 30 min and centrifuged at 2380 RCF for 30 min to obtain single-to-few-layered MXene flakes. The final suspension of $Ti_3C_2T_x$ MXene was collected and stored in the freezer at −20 °C until use. The $Ti_3C_2T_x$ MXene dispersions of varying concentrations were prepared in deionized water using probe sonication (Fisherbrand Model 120 Sonic Dismembrator) for 30 min at a 90% amplitude. The flake size distribution of $Ti_3C_2T_x$ MXene investigated using a zetasizer Nano ZS, Malvern Instruments is shown in Figure 1b. The average flake size of $Ti_3C_2T_x$ MXene was 4.56 ± 0.38 μm. The specific details of $Ti_3C_2T_x$ MXene flake size characterization and validation using SEM are reported in our previous study.[34] Furthermore, $Ti_3C_2T_x$ MXene/DI water solutions at MXene concentrations 0.05, 0.1, 0.2, and 0.5 wt % were prepared by adding the required amount of DI water. The phase purity of the prepared $Ti_3C_2T_x$ MXene samples was confirmed by X-ray diffraction analysis and reported in Figure S1 of Supporting

https://doi.org/10.1021/acsomega.4c06988
ACS Omega 2025, 10, 6534−6543

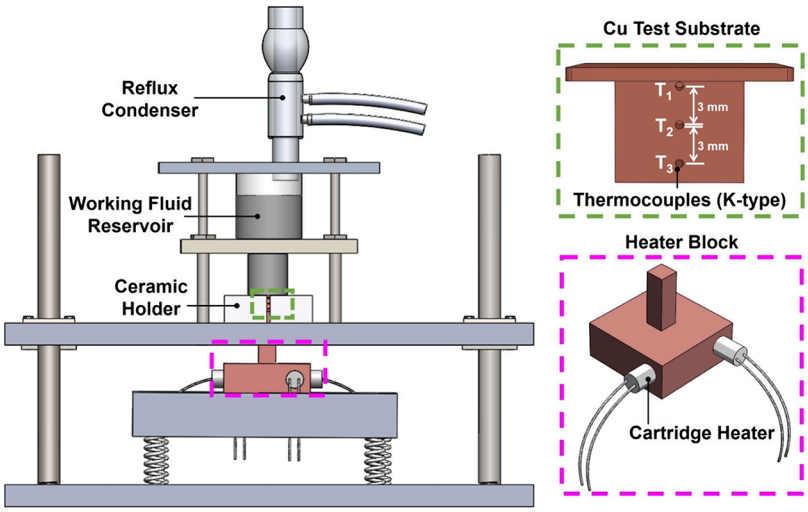

Figure 2. Schematic of the pool boiling setup along with thermocouple location for temperature measurements.

Information. Extensive characterization of MXene dispersions have been previously reported by Thakur et al.[34] provide an in-depth analysis of MXene flake properties, including size distributions, morphology, and surface chemistry.

The viscosities of $Ti_3C_2T_x$ MXene dispersions were measured using a NETZSCH-Geräte bau GmbH Kinexus Ultra+ rotational rheometer with a 50 mm, 0.1° cone and plate attachment at shear rates $\dot{\gamma}$ between 0.1 and 100 s^{-1} and at room temperature. Reference viscosity values for water at various temperatures were used to calibrate the rheometer. The measurement error was estimated by calculating the maximum deviation between these reference values and the actual measured values for deionized water. For concentrations up to 0.5 wt %, no measurable shear rate dependencies were observed so values of viscosity reported here were for a single shear rate $\dot{\gamma} = 5\ s^{-1}$, where the results were observed to be most stable, and the maximum error estimate was ±4%.

2.2. Boiling Setup. The details of the pool boiling setup and validation have been previously reported by our group.[35] Uncertainty analysis is summarized in SI. Briefly, the test section includes a ceramic chip holder used to secure the copper test chip, which is supported by a bottom Garolite plate. A quartz glass water reservoir (14 × 14 × 38 mm) is placed on top of the test chip, with a rubber gasket sealing the interface between the test chip and the reservoir, extending beyond the 10 × 10 mm boiling surface as shown in Figure 2. Kapton tape with a thermal conductivity of 0.2 W/m °C is applied to provide additional coverage for the excess area. The working fluid reservoir is mounted on a Garolite plate and fastened to the top aluminum plate using socket head cap screws. Temperature measurements are recorded using a National Instruments cDAQ-9172 data acquisition system equipped with a NI-9213 thermocouple input module. All the boiling experiments are conducted using deionized water and $Ti_3C_2T_x$ MXene dispersions with varying concentrations under atmospheric pressure conditions within an open-loop system, with a reflux condenser. Heat flux was calculated using eqs 1 and 2:

$$q'' = -k_{Cu}(dT/dx) \tag{1}$$

$$\frac{dT}{dx} = \frac{3T_1 - 4T_2 + T_3}{2\Delta x} \tag{2}$$

The temperature gradient shown in eq 2 is derived in SI. Surface temperature (T_{wall}) and HTC were quantified using eqs 3 and 4:

$$T_{wall} = T_1 - q''(x_1/k_{Cu}) \tag{3}$$

$$\text{HTC} = \frac{q''}{T_{wall} - T_{sat}} \tag{4}$$

T_{sat} is the saturation temperature of the working liquid and k_{Cu} is the thermal conductivity of the copper substrate. Each boiling run was triplicated and a yielded minimal error of 5%.

2.3. Surface Characterization. The surface topography of the heated surface after pool boiling tests was analyzed using a Keyence VHX-600 digital microscope and a HITACHI S-4800 high-resolution scanning electron microscope (SEM) with 1 nm spatial resolution at an accelerated voltage of 20 kV using both secondary electrons and backscattered electron detectors. The energy dispersive X-ray spectroscopy (EDS) measurements were performed using a 50 mm^2 Oxford Silicon Drift detector attached to the HITACHI S-4800 SEM 3D topography mapping was performed on a Keyence VHX-600 digital microscope. Additionally, the static contact angles (SCA) of the surfaces were measured using the sessile drop method on a Nanoscience Instruments Theta Lite Optical Tensiometer. This instrument was equipped with an auto sample dispenser and a camera, enabling precise measurement of the contact angles.

3. RESULTS AND DISCUSSION

The stability of dispersions plays a critical role in enhancing heat transfer efficiency by ensuring uniform distribution of additives and prevention of their agglomeration. For long-term use and maintenance of heat exchanging systems, it is particularly advantageous to maintain the stability of heat exchange fluids comparison of additives allowing for reversible redispersion without substantial degradation of additives.[30] This combination of stability and reversibility is crucial for optimizing performance and extending the lifespan of heat transfer systems. Concentration-dependent rheology is another factor for heat-exchanging fluid applications, as it allows for the tuning of viscosity and flow properties to optimize heat transfer efficiency and pumping power requirements.[36] Therefore, it was imperative to maintain the viscosity of a dispersion close to

https://doi.org/10.1021/acsomega.4c06988
ACS Omega 2025, 10, 6534−6543

that of the water.[37] The stability of the $Ti_3C_2T_x$ MXene dispersions were evaluated by monitoring the dispersions stored at room temperatures. The images of freshly prepared dispersions and dispersions that were left untouched for 96 h are shown in Figure 3a that show no changes in concentration,

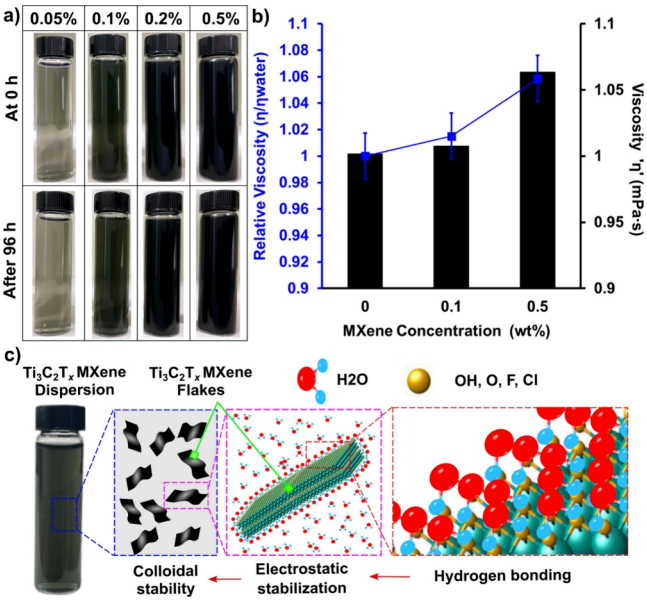

Figure 3. (a) Photographic images of freshly prepared MXene dispersions after 96 h. (b) Relative viscosities (blue) and shear viscosities (black) of $Ti_3C_2T_x$ *MXene dispersions at room temperature. Reported values assessed at a shear rate* $\dot{\gamma} = 5\ s^{-1}$*; error bars are based on the maximum deviation, (c) schematic of stabilization mechanism of* $Ti_3C_2T_x$ *MXene dispersion.*

agglomeration, and sedimentation of $Ti_3C_2T_x$ MXene. This is attributed to the abundant hydrophilic, negatively charged terminal functional groups on their surface forming hydrogen bonds with water molecules resulting in electrostatic stabilization, allowing for the formation of stable colloidal aqueous solutions without the need for surfactants or polymers as shown in Figure 3c.[38] Figure 3b compares the measured relative viscosity of 0.1 and 0.5 wt % $Ti_3C_2T_x$ MXene with water at room temperature. The addition of 0.1 wt % $Ti_3C_2T_x$ MXene showed a negligible impact on viscosity, with an average increase of only 1.4%, which is well within the margin of error. In contrast, at 0.5 wt % $Ti_3C_2T_x$ MXene, the viscosity increased by an average of 6.3% across all temperatures. This rise in viscosity can be attributed to the higher flake concentration of $Ti_3C_2T_x$ MXene, leading to increased internal friction and interface resistance to flow. The single-to-few layer flake morphologies of $Ti_3C_2T_x$ MXenes, characterized by larger flake sizes and aspect ratios, likely contributed to this viscosity increase. Previous studies have shown that variations in flake size and concentration can result in viscosity changes ranging from 4 to 15% to as much as 50%, depending on the nanoparticle concentration.[39−41]

The excellent colloidal stability of $Ti_3C_2T_x$ MXene dispersions, as evidenced by our stability studies, is crucial for heat-exchanging fluids. Stable dispersions prevent agglomeration and sedimentation, ensuring consistent performance over time and maintaining enhanced thermal properties throughout the heat exchange system.[42] Additionally, rheological studies exhibited a minimal increase in viscosity compared to the base fluid. This is advantageous for heat-exchanging fluids as it maintains good flow characteristics, minimizing the additional pumping power required while still providing enhanced thermal properties.[43] The pool boiling performance of $Ti_3C_2T_x$ MXene dispersions at concentrations of 0.05, 0.1, and 0.2 wt % was investigated and compared to DI water. Figure 4a illustrates the relationship between heat flux

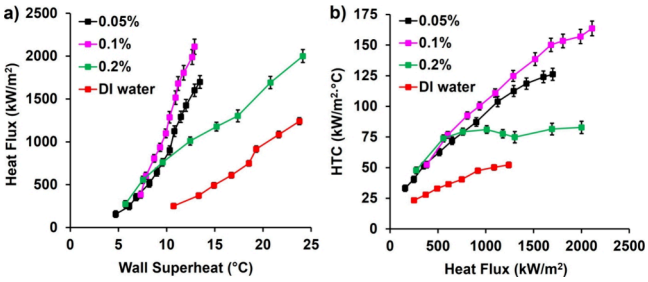

Figure 4. Boiling performance of $Ti_3C_2T_x$ *MXene dispersions compared to deionized water (a) Heat flux vs wall super heat, (b) Heat transfer coefficient (HTC) vs heat flux.*

and wall superheat for the various MXene dispersion concentrations and DI water. In this context, the critical heat flux (CHF) represents the maximum heat transfer achievable before the formation of an insulating vapor layer on the heater surface. This vapor layer, once formed, prevents rewetting, and impairs heat transfer efficiency.[57] The CHF, therefore, serves as a crucial indicator of the maximum heat dissipation capacity of the MXene-enriched boiling fluid. Figure 4b presents the heat transfer coefficient (HTC), a key metric of heat transfer efficiency. The HTC was calculated as the ratio of heat flux to wall superheat, using the data obtained from Figure 4a.

The $Ti_3C_2T_x$ MXene dispersions exhibited noticeable higher CHF values at lower wall superheats compared to DI water. All dispersion concentrations demonstrated enhanced CHF compared to DI water, with the 0.1 wt % $Ti_3C_2T_x$ MXene dispersion achieving the highest CHF improvement by 70% at a low WS of 12 °C. The presence of 0.2 wt % MXene flakes yielded a similar critical heat flux as 0.1 wt %, however, the wall superheat was around 25 °C like that of DI water. While 0.05 wt % MXene dispersion produced a low wall superheat of 12 °C same as that of 0.1 wt %, but at a lower CHF. Thus, the 0.1 wt % concentration emerged as the optimal formulation, striking an ideal balance between maximizing CHF and minimizing wall superheat, suggesting that carefully tuning the MXene concentration is crucial for optimizing pool boiling performance.

The comparison of heat flux and HTC presented in Figure 4b further confirms the superior boiling heat transfer performance of 0.1 wt % $Ti_3C_2T_x$ MXene dispersion. It is important to note that enhanced CHF does not always coincide with improved HTC. Higher values of HTC obtained with MXene indicate their ability to absorb more heat from the surface for a given temperature difference, thereby enhancing the cooling performance of the system. Several studies have reported a deterioration in HTC with an increase in nanoparticle concentration.[13,44,45] This is often attributed to the formation of a thick nanoparticle deposit layer on the heated surface, which can increase the surface's thermal resistance and negatively impact its heat transfer. However, in case of $Ti_3C_2T_x$ MXene dispersions, both CHF and HTC were enhanced.

The boiling of MXene dispersions resulted in alteration of the heater surface characteristics, primarily due to the deposition of MXene flakes. WE investigated this phenomenon

https://doi.org/10.1021/acsomega.4c06988
ACS Omega 2025, 10, 6534−6543

using advanced analytical techniques, including scanning electron microscopy (SEM) and goniometry. Figure 5a−c

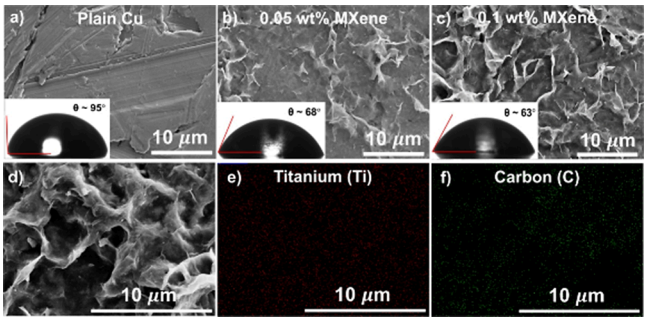

Figure 5. Scanning electron microscopy and contact angle measurement of (a) plain copper surface, (b, c) surface post boiling of 0.05 and 0.1 wt % MXene dispersion, (d−f) Ti and C elemental mapping of MXene deposited heater surface.

presents SEM images of plain copper vs samples with 0.05 and 0.1 wt % MXene. Comparing the surfaces in these images provides evidence of $Ti_3C_2T_x$ MXene flake deposition on the copper heater surface. These images reveal distinct changes in surface topography following the boiling experiments with 0.05 and 0.1 wt % $Ti_3C_2T_x$ MXene dispersions, compared to the plain copper surface. Accompanying the topographical changes, significant alterations in surface wettability were observed, as evidenced by the contact angle measurements shown in the inset images of Figure 5a−c. The plain copper heater surface initially exhibited a contact angle of 95°, indicating a relatively hydrophobic nature. However, after boiling with the 0.1 wt % $Ti_3C_2T_x$ MXene dispersion, the contact angle decreased dramatically to 63°. This substantial reduction in contact angle demonstrates enhanced hydrophilicity of the surface following $Ti_3C_2T_x$ MXene deposition.

To further characterize the surface modification resulting from MXene deposition, elemental mapping analysis was performed on the 0.1 wt % MXene surface post boiling test shown in Figure 5d. Figure 5e illustrates the spatial distribution of titanium (Ti), while Figure 5e shows the carbon (C) distribution across the analyzed area. The presence and colocalization of these elements are characteristic signatures of $Ti_3C_2T_x$ MXene flakes. Further evidence of surface modification due to MXene deposition is presented in Figure S2 of the Supporting Information. This figure includes additional static water contact angle measurements and microscopic images of copper substrates following boiling experiments with various $Ti_3C_2T_x$ MXene concentrations. It was observed that increasing the $Ti_3C_2T_x$ MXene concentration from 0.1 to 0.2 wt % led to an unexpected increase in static contact angles suggesting a nonlinear relationship between $Ti_3C_2T_x$ MXene concentration and surface wettability. This trend indicates that an optimal concentration exists for maximizing hydrophilicity, beyond which the surface properties begin to change differently.

The enhanced CHF and HTC observed with a thinner MXene deposition layer can be attributed to the unique properties of $Ti_3C_2T_x$ MXene flakes. These characteristics include the concentration of $Ti_3C_2T_x$ MXene in the fluid, the size and aspect ratio of individual flakes, and their negative surface charges. These specific attributes of $Ti_3C_2T_x$ MXene flakes contribute to considerable changes in the heat transfer process, particularly by altering surface wettability through the deposition of MXene flakes on the copper substrate. The $Ti_3C_2T_x$ MXene-deposited heater surface revealed a notably rough and textured topography showing $Ti_3C_2T_x$ MXene flakes forming a complex, hierarchical structure on the heater surface observed as protrusions,[46] cavities,[47] and interconnected networks[48] of MXene flakes that play a crucial role in enhancing the boiling process. The rough texture created by the deposited MXene flakes can increase the number of potential nucleation sites on the heater surface for the formation of vapor bubbles. Moreover, the interconnected nature of the deposited MXene flakes can create a porous network on the surface that not only offers additional nucleation sites but also facilitates liquid replenishment to the heating surface through capillary wicking. Such enhanced liquid supply can delay the onset of dry-out conditions, contributing to the observed improvements in CHF. The combination of increased nucleation site density and improved liquid replenishment mechanisms explains, in part, the superior boiling performance of MXene-deposited surfaces.

Mechanistically, the enhanced boiling performance of $Ti_3C_2T_x$ MXene dispersions is attributed to the synergistic effects of thermophoretic-Brownian motion and stratification phenomena shown schematically in Figure 6. The scanning

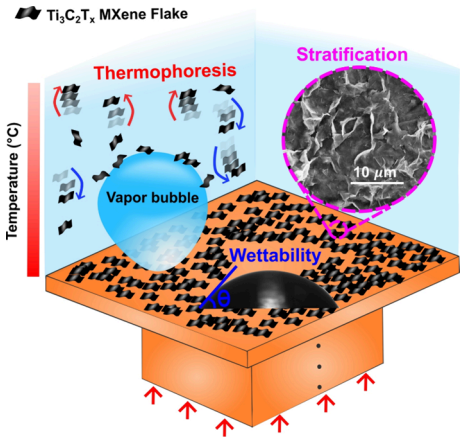

Figure 6. Schematic representation of proposed thermophoresis, stratification, and wetting mechanisms responsible for $Ti_3C_2T_x$ *MXene dispersion boiling enhancement along with SEM of* $Ti_3C_2T_x$ *MXene flakes deposited on Cu substrate.*

electron microscope (SEM) image shown in Figure 5 confirms the flake-like deposition of $Ti_3C_2T_x$ MXenes on the copper heater substrate after the boiling experiment. In the context of nanofluids, researchers have reported that heat transfer is enhanced by the increased Brownian motion of nanoparticles. This motion, which is driven by thermophoretic forces, leads to two important effects: it promotes more frequent collisions between particles, and it helps create a more uniform temperature distribution within the fluid's boundary layer. These combined effects contribute to the overall improvement in heat transfer observed in nanofluid systems. The thermophoretic mobility of the nanoparticles is represented by the thermophoretic velocity as,

$$V_T = -D_T \nabla T \tag{5}$$

where D_T is the thermophoretic diffusion coefficient and ∇T is the temperature gradient.[49,50] Concurrently, the Brownian motion of flakes due to their collision with fluid molecules, helps disperse the flakes in the bulk fluid and contributes to the stratification of the flakes forming a layer on the heated

https://doi.org/10.1021/acsomega.4c06988
ACS Omega 2025, 10, 6534−6543

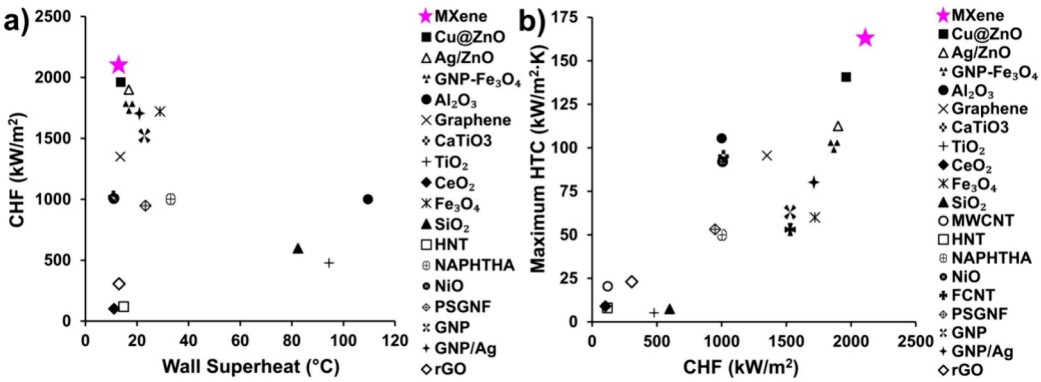

Figure 7. Comparison of $Ti_3C_2T_x$ *MXene dispersion performance with literature reported dispersions, (a) CHF vs WS, (b) maximum HTC vs CHF. Nanofluids: Graphene,*[77] *TiO_2,*[78] *Al_2O_3,*[79] *CeO_2,*[80] *Fe_3O_4,*[15] *SiO_2,*[17] *Cu@ZnO,*[69] *Ag/ZnO,*[16] *HNT,*[81] *NAPHTHA,*[82] *$CaTiO_3$,*[83] *NiO,*[83] *PSGNF,*[84] *GNP,*[20] *GNP/Ag,*[20] *rGO,*[85] *GNP-Fe_3O_4,*[20] *MWCNT,*[86] *FCNT.*[45]

surface.[51,52] Subsequently, the formation of concentration gradients, or stratification, in the dispersion alters surface wettability and nucleation site density.[53,54] The thermophoretic behavior and its influence on thermal conductivity enhancement can differ between dispersions containing spherical nanoparticles versus those with flake-like particles due to the differences in particle shape, orientation, and interaction with the surrounding medium.[27,55] For flake-like morphology, such as those of $Ti_3C_2T_x$ MXene, the orientation and shape of the flakes can influence their thermophoretic behavior, in addition to the temperature gradient. The impact of thermophoresis on the distribution of $Ti_3C_2T_x$ MXene flakes in the dispersion can be more pronounced compared to spherical particles, and these thermophoretic effects become more pronounced as the $Ti_3C_2T_x$ MXene flake concentration increases.[56] The thermophoretic force arises due to temperature gradients, resulting in an uneven transfer of momentum from the fluid molecules to the flake surface. With increasing flake concentrations, a greater number of flakes experience uneven momentum transfer, amplifying the thermophoretic effect. The increased thermophoretic velocity at higher $Ti_3C_2T_x$ MXene flake concentrations results in a more pronounced migration of the flakes from the hot region to the cold region within the dispersion.[57−61]

Furthermore, macrolayer dryout theory, suggests that a lower contact angle, indicating better surface wettability, may have contributed to the observed higher CHF. The model assumes that the bubbles stay above the heated surface for a significant period before departing, and these bubbles are separated from the surface by a liquid microlayer. When the heat flux is high enough to evaporate this microlayer before the bubble departs, the CHF is reached, leading to a sudden rise in surface temperature. The research indicates that the deposition of nanoparticles on the heated surface can lead to a decrease in the contact angle, which in turn increases the thickness of the microlayer, which results in a macrolayer. The resultant macrolayer thickness as a function of bubble radius, as predicted by the Sadasivan et al. model, can delay the macrolayer dryout and lead to an enhancement in the CHF for dispersions compared to the base fluid.[62]

The influence of dispersions on bubble departure diameter and frequency, crucial factors affecting heat transfer coefficients, varies based on the specific nanoparticle material, size, and concentration employed in the system. Additives and particles can accumulate around the bubbles, shown schematically in Figure 6, similar to how surfactants behave, and modify the surface tension[63] When nanoparticles cluster around bubbles, they can hinder bubble growth and increase the nanoparticle agglomeration in the fluid wedge. This nanoparticle deposition pattern modifies the surface roughness and accelerates the sweeping mechanism of vapor bubbles that involves back-and-forth movement of bubbles along the heating surface which may further enhance mixing and heat transfer.[64] Thus, the addition of nanoparticles or additives to the base fluid can alter the liquid−vapor interface properties, intensifying the bubble dynamics by increasing the number of active nucleation sites, allowing for more efficient bubble formation and departure, thereby enhancing heat transfer.[26,65,66]

The study of bubble dynamics, such as bubble growth, departure, and frequency, plays a crucial role in determining the overall boiling heat transfer characteristics. However, due to the poor optical properties of $Ti_3C_2T_x$ MXene dispersions, the use of high-speed cameras to capture the bubble dynamics during pool boiling was challenging, and therefore, not reported. This limitation in experimental visualization made it difficult to directly measure bubble radius and correlate them to develop empirical models for pool boiling heat transfer of $Ti_3C_2T_x$ MXene dispersions. This limitation has been acknowledged in the study, and the authors suggest that future work should focus on overcoming this challenge through theoretical modeling or simulation. This could involve developing mathematical models that describe the behavior of bubbles in the presence of $Ti_3C_2T_x$ MXene, considering factors such as surface tension, contact angle, and the interaction between the $Ti_3C_2T_x$ MXene flakes and the liquid−vapor interface. Another approach to overcoming the limitation is to use computational fluid dynamics (CFD) that can provide a detailed, quantitative analysis of the bubble formation, growth, and detachment processes, as well as the heat transfer characteristics of the boiling process. Alternatively, using X-ray or neutron imaging techniques can provide noninvasive, high-resolution imaging of the bubble behavior inside the dispersion, overcoming the limitations of optical imaging.[67,68]

Figure 7a,b compares the boiling heat transfer performance of $Ti_3C_2T_x$ MXene dispersions with various nanofluids reported in the literature for pool boiling. The $Ti_3C_2T_x$ MXene dispersion performance was closely followed by the Cu@ZnO nanofluid, which was tested on copper microchannels rather than a plain copper surface.[69] The $Ti_3C_2T_x$ MXene flakes, being composed of titanium carbide, yielded higher CHF and HTC values compared to titanium oxide (TiO_2) nanofluids. This can be attributed to the nonspherical

https://doi.org/10.1021/acsomega.4c06988
ACS Omega 2025, 10, 6534−6543

shape of the $Ti_3C_2T_x$ MXene flakes, the presence of carbon atoms in their structure, and the high thermal conductivity of $Ti_3C_2T_x$ MXene 55.8 W/m °C,[33] compared to TiO_2 nanoparticle thermal conductivity of 8.5 W/m °C.[70] $Ti_3C_2T_x$ MXene also exhibited superior boiling performance compared to commonly used low thermally conductive nanoparticles such as Fe_2O_3 at 6 W/m °C,[71] Al_2O_3 at 40 W/m °C,[72] and SiO_2 at 10.4 W/m °C.[73] Furthermore, the $Ti_3C_2T_x$ MXene dispersions also surpassed the boiling heat transfer performance of carbon-rich nanofluids with high thermally conductive nanomaterials, including those comprised of graphene with 3000 W/m °C,[74] graphene nanoplatelets (GNP) with 4000 W/m °C,[75] and multiwalled carbon nanotubes (MWCNT) with 6150 W/m °C.[76] Based on this observation, we hypothesize that the addition of highly thermally conductive nanomaterials is not the only factor that impacts the pool boiling performance. The enhancement in pool boiling performance is a combination of multiple factors that come into play during pool boiling.

The superior pool boiling performance of $Ti_3C_2T_x$ MXene dispersions stem from a confluence of factors, encompassing the nanoparticle shape, concentration, and rheological attributes of the dispersion composition. The incorporation of $Ti_3C_2T_x$ MXene flakes elevates the thermal conductivity of the base fluid, promoting efficient heat transfer mechanisms. Moreover, the presence of $Ti_3C_2T_x$ MXene flakes on the heated surface during boiling induces alterations in interfacial properties, such as surface roughness, fostering the creation of additional nucleation sites for enhanced bubble dynamics. Furthermore, the enhanced wettability of the heated surface facilitated by $Ti_3C_2T_x$ MXene flakes, as indicated by reduced contact angles, promotes the formation of a thin liquid film, delaying the critical heat flux onset and augmenting the heat transfer coefficient. The collective enhancements in thermal conductivity, surface roughness, and wettability collectively contribute to the notable enhancements in both critical heat flux and heat transfer coefficient observed with $Ti_3C_2T_x$ MXene dispersions compared to deionized water.

4. CONCLUSIONS

MXenes, an emerging family of two-dimensional nanomaterials, have recently gained notable attention in the field of thermal management and energy applications. This study investigates the potential of 2D $Ti_3C_2T_x$ MXene in pool boiling heat transfer, demonstrating substantial enhancements in both critical heat flux (CHF) and heat transfer coefficient (HTC) compared to deionized (DI) water. At an optimal concentration of 0.1 wt %, $Ti_3C_2T_x$ MXene dispersions exhibited remarkable improvements of approximately 70% in CHF and 213% in HTC relative to DI water. These enhancements are attributed to three key factors: (1) increased nucleation site density, (2) the heterogeneous nature of the surface due to stratification or layering of particles, and (3) increased wettability. The unique surface interactions of $Ti_3C_2T_x$ MXene flakes form a thin deposition layer on the heated surface during boiling, creating a nanoscale coating that leads to an increase in active nucleation sites and improved boiling heat transfer efficiency. The stratified layer of MXene particles creates a heterogeneous surface topology, further contributing to enhanced heat transfer performance. Additionally, the increased wettability induced by the MXene coating plays a crucial role in improving both CHF and HTC. Notably, these performance gains were achieved without significantly altering the fluid's viscosity, highlighting the potential of $Ti_3C_2T_x$ MXene dispersions for practical thermal management solutions. The tunable rheological properties of MXene dispersions, coupled with their exceptional heat transfer capabilities, position them as promising candidates for advanced thermal applications, including next-generation heat exchangers, high-performance cooling systems, and innovative thermal energy storage devices.

■ ASSOCIATED CONTENT

Supporting Information

The Supporting Information is available free of charge at https://pubs.acs.org/doi/10.1021/acsomega.4c06988.

X-ray diffraction (XRD) analysis of $Ti_3C_2T_x$ MXene, uncertainty propagation analysis of boiling experiment, surface, and static contact angle analysis (PDF)

■ AUTHOR INFORMATION

Corresponding Author

Anju Gupta − *Department of Mechanical, Industrial and Manufacturing Engineering, The University of Toledo, Toledo, Ohio 43606, United States;* orcid.org/0000-0001-5378-9496; Phone: +1 (413) 530-8213; Email: anju.gupta@utoledo.edu

Authors

Saketh Merugu − *Department of Mechanical, Industrial and Manufacturing Engineering, The University of Toledo, Toledo, Ohio 43606, United States*

Md Moynul Hasan − *Department of Mechanical, Industrial and Manufacturing Engineering, The University of Toledo, Toledo, Ohio 43606, United States*

Anupma Thakur − *School of Materials Engineering, Purdue University, West Lafayette, Indiana 47907, United States*

Jacob Patenaude − *School of Mechanical Engineering, Purdue University, West Lafayette, Indiana 47907, United States*

Babak Anasori − *School of Materials Engineering and School of Mechanical Engineering, Purdue University, West Lafayette, Indiana 47907, United States;* orcid.org/0000-0002-1955-253X

George Choueiri − *Department of Mechanical, Industrial and Manufacturing Engineering, The University of Toledo, Toledo, Ohio 43606, United States*

Complete contact information is available at: https://pubs.acs.org/10.1021/acsomega.4c06988

Author Contributions

S.M.: investigation, visualization, data curation, formal analysis, and writing−original draft. M.M.H.: investigation. A.T.: methodology and investigation. J.P.: review, editing, and discussion. B.A.: methodology, supervision, and writing−review and editing. G.C.: investigation. A.G.: conceptualization, project administration, supervision, and writing−review and editing.

Notes

The authors declare no competing financial interest.

■ ACKNOWLEDGMENTS

A.G. and S.M. would like to acknowledge the US National Science Foundation (NSF) (Award #CBET- 2002310) for financial support for MXene electron microscopy. A.T. and

B.A. acknowledge funding support from the US National Science Foundation (Award #CMMI-2134607).

ABBREVIATION AND NOMENCLATURE

CHF, critical heat flux (kW/m^2)
HTC, heat transfer coefficient (kW/m^2 °C)
q'', heat flux (kW/m^2)
∇T, temperature gradient (K/m)
k_{Cu}, thermal conductivity of copper (W/m °C)
V_T, thermophoretic velocity (ms^{-1})
D_T, thermophoretic diffusion coefficient (m^2/s K)
SCA, static contact angle (°)
T_{wall}, surface temperature of the copper substrate (°C)
T_{sat}, saturation temperature of working liquid (°C)
ΔT, wall superheat (°C)
WS, wall superheat (°C)

REFERENCES

(1) Timofeeva, E. V.; Yu, W.; France, D. M.; Singh, D.; Routbort, J. L. Nanofluids for heat transfer: an engineering approach. *Nanoscale Res. Lett.* **2011**, *6*, 182.
(2) Kiani, M.; Omiddezyani, S.; Houshfar, E.; Miremadi, S. R.; Ashjaee, M.; Nejad, A. M. Lithium-ion battery thermal management system with Al2O3/AgO/CuO nanofluids and phase change material. *Appl. Therm. Eng.* **2020**, *180*, No. 115840.
(3) Devarajan, Y.; Munuswamy, D. B. Analysis on the influence of nanoparticles of alumina, copper oxide, and zirconium oxide on the performance of a flat-plate solar water heater. *Energy Fuels* **2016**, *30* (11), 9908−9913.
(4) Jaikumar, A.; Kandlikar, S. G. Enhanced pool boiling for electronics cooling using porous fin tops on open microchannels with FC-87. *Applied Thermal Engineering* **2015**, *91*, 426−433.
(5) Ma, X.; Song, G.; Chen, H.; Zhang, Y.; Xu, N.; Wei, J. Experimental investigation and correlation analysis of pool boiling heat transfer on the array surfaces with micro-fins using FC-72 for the electronic thermal management. *Applied Thermal Engineering* **2024**, *236*, No. 121755.
(6) Rajaram, K.; Raman, M.; Dhanapal, K.; Muthusamy, S.; Ramamoorthi, P.; Govindasamy, M.; Mishra, O. P. Nucleate pool boiling thermal management systems of hydrazine reduced graphene oxide (H-rGO) nanofluids with rough surface. *Energy Sources, Part A: Recovery, Utilization, and Environmental Effects* **2023**, *45* (3), 6994−7007.
(7) Azizian, R.; Doroodchi, E.; Moghtaderi, B. Effect of nano-convection caused by Brownian motion on the enhancement of thermal conductivity in nanofluids. *Industrial & engineering chemistry research* **2012**, *51* (4), 1782−1789.
(8) Solangi, K.; Kazi, S.; Luhur, M.; Badarudin, A.; Amiri, A.; Sadri, R.; Zubir, M.; Gharehkhani, S.; Teng, A. H. A comprehensive review of thermo-physical properties and convective heat transfer to nanofluids. *Energy* **2015**, *89*, 1065−1086.
(9) Akbari, A.; Mohammadian, E.; Alavi Fazel, S. A.; Shanbedi, M.; Bahreini, M.; Heidari, M.; Ahmadi, G. Comparison between nucleate pool boiling heat transfer of graphene nanoplatelet-and carbon nanotube-based aqueous nanofluids. *Acs Omega* **2019**, *4* (21), 19183−19192.
(10) Chavali, M. S.; Nikolova, M. P. Metal oxide nanoparticles and their applications in nanotechnology. *SN Appl. Sci.* **2019**, *1* (6), 607.
(11) Kapil, N.; Mayani, S. V.; Bhattacharyya, K. G. Environmental implications of nanoceramic applications. *Results in Chemistry* **2023**, *5*, No. 100724.
(12) Wen, T.; Luo, J.; Jiao, K.; Lu, L. Experimental study on the pool boiling performance of a highly self-dispersion TiO_2 nanofluid on copper surface. *International Journal of Thermal Sciences* **2023**, *184*, No. 107999.
(13) Pare, A.; Ghosh, S. K. The empirical characteristics on transient nature of Al_2O_3-water nanofluid pool boiling. *Applied Thermal Engineering* **2021**, *199*, No. 117617.
(14) Cheedarala, R. K.; Song, J. I. Face-centred cubic CuO nanocrystals for enhanced pool-boiling critical heat flux and higher thermal conductivities. *Int. J. Heat Mass Transfer* **2020**, *162*, No. 120391.
(15) Du, J.; Yang, W.; Zhu, H.; Wang, J.; Cao, Z.; Sundén, B. Experimental study of pool boiling performance of Fe_3O_4 ferromagnetic nanofluid on a copper surface. *Applied Thermal Engineering* **2024**, *248*, No. 123213.
(16) Sharma, P. O.; Barewar, S. D.; Chougule, S. S. Experimental investigation of heat transfer enhancement in pool boiling using novel Ag/ZnO hybrid nanofluids. *J. Therm. Anal. Calorim.* **2021**, *143*, 1051−1061.
(17) Wang, S.; Hsieh, H.-E.; Zhang, Z.; Wang, S.; Cai, X. CHF and heat transfer enhancement by SiO_2 nanofluids on a inclined downward facing heating surface. *Prog. Nucl. Energ* **2024**, *171*, No. 105197.
(18) Rishi, A. M.; Kandlikar, S. G.; Rozati, S. A.; Gupta, A. Effect of ball milled and sintered graphene nanoplatelets−copper composite coatings on bubble dynamics and pool boiling heat transfer. *Adv. Eng. Mater.* **2020**, *22* (7), No. 1901562.
(19) Rishi, A. M.; Kandlikar, S. G.; Gupta, A. Salt templated and graphene nanoplatelets draped copper (GNP-draped-Cu) composites for dramatic improvements in pool boiling heat transfer. *Sci. Rep.* **2020**, *10* (1), 11941.
(20) Ma, X.; Song, Y.; Wang, Y.; Zhang, Y.; Xu, J.; Yao, S.; Vafai, K. Experimental study of boiling heat transfer for a novel type of GNP-Fe_3O_4 hybrid nanofluids blended with different nanoparticles. *Powder Technol.* **2022**, *396*, 92−112.
(21) Inbaoli, A.; Kumar, C. S.; Jayaraj, S. A review on techniques to alter the bubble dynamics in pool boiling. *Appl. Therm. Eng.* **2022**, *214*, No. 118805.
(22) Mehralizadeh, A.; Shabanian, S. R.; Bakeri, G. Effect of modified surfaces on bubble dynamics and pool boiling heat transfer enhancement: A review. *Therm. Sci. Eng. Prog.* **2020**, *15*, No. 100451.
(23) Modi, M.; Kangude, P.; Srivastava, A. Performance evaluation of alumina nanofluids and nanoparticles-deposited surface on nucleate pool boiling phenomena. *Int. J. Heat Mass Transfer* **2020**, *146*, No. 118833.
(24) Pare, A.; Ghosh, S. K. The chronological study on parametric evolution of pool boiling with nanofluids: An experimental review. *Therm. Sci. Eng. Prog.* **2022**, *34*, No. 101420.
(25) Akbari, E.; Holagh, S. G.; Saffari, H.; Shafiee, M. On the effect of silver nanoparticles deposition on porous copper foams on pool boiling heat transfer enhancement: an experimental visualization. *Heat and Mass Transfer* **2022**, *58* (3), 447−466.
(26) Kim, H. Enhancement of critical heat flux in nucleate boiling of nanofluids: a state-of-art review. *Nanoscale Res. Lett.* **2011**, *6*, 415.
(27) Maheshwary, P.; Handa, C.; Nemade, K. A comprehensive study of effect of concentration, particle size and particle shape on thermal conductivity of titania/water based nanofluid. *Applied Thermal Engineering* **2017**, *119*, 79−88.
(28) Rahman, M. A.; Hasnain, S. M.; Pandey, S.; Tapalova, A.; Akylbekov, N.; Zairov, R. Review on Nanofluids: Preparation, Properties, Stability, and Thermal Performance Augmentation in Heat Transfer Applications. *Acs Omega* **2024**, *9*, 32328.
(29) Ouyang, T.; Liu, B.; Wang, C.; Ye, J.; Liu, S. Novel hybrid thermal management system for preventing Li-ion battery thermal runaway using nanofluids cooling. *Int. J. Heat Mass Transfer* **2023**, *201*, No. 123652.
(30) Panduro, E. A. C.; Finotti, F.; Largiller, G.; Lervåg, K. Y. A review of the use of nanofluids as heat-transfer fluids in parabolic-trough collectors. *Appl. Therm. Eng.* **2022**, *211*, No. 118346.
(31) Mukherjee, S.; Ebrahim, S.; Mishra, P. C.; Ali, N.; Chaudhuri, P. A review on pool and flow boiling enhancement using nanofluids: Nuclear reactor application. *Processes* **2022**, *10* (1), 177.

https://doi.org/10.1021/acsomega.4c06988
ACS Omega 2025, 10, 6534−6543

(32) Naguib, M.; Kurtoglu, M.; Presser, V.; Lu, J.; Niu, J.; Heon, M.; Hultman, L.; Gogotsi, Y.; Barsoum, M. W. Two-dimensional nanocrystals produced by exfoliation of Ti3AlC2. In *MXenes*; Jenny Stanford Publishing: 2011; pp 15−29.
(33) Liu, R.; Li, W. High-thermal-stability and high-thermal-conductivity Ti3C2T x MXene/poly (vinyl alcohol)(PVA) composites. *Acs Omega* **2018**, *3* (3), 2609−2617.
(34) Thakur, A.; Chandran, B. S. N.; Davidson, K.; Bedford, A.; Fang, H.; Im, Y.; Kanduri, V.; Wyatt, B. C.; Nemani, S. K.; Poliukhova, V.; et al. Step-by-step guide for synthesis and delamination of $Ti_3C_2T_x$ MXene. *Small Methods* **2023**, *7* (8), No. 2300030.
(35) Rozati, S. A.; Keesara, P.; Mahajan, C.; Mondal, K.; Gupta, A. Magnetically aligned metal-organic deposition (MOD) ink based nickel/copper heater surfaces for enhanced boiling heat transfer. *Appl. Therm. Eng.* **2022**, *211*, No. 118473.
(36) Siddique, I.; Abdal, S.; Din, I. S. U.; Awrejcewicz, J.; Pawłowski, W.; Hussain, S. Significance of concentration-dependent viscosity on the dynamics of tangent hyperbolic nanofluid subject to motile microorganisms over a non-linear stretching surface. *Sci. Rep.* **2022**, *12* (1), 12765.
(37) Soman, D. P.; Karthika, S.; Kalaichelvi, P.; Radhakrishnan, T. Impact of viscosity of nanofluid and ionic liquid on heat transfer. *J. Mol. Liq.* **2019**, *291*, No. 111349.
(38) Maleski, K.; Mochalin, V. N.; Gogotsi, Y. Dispersions of two-dimensional titanium carbide MXene in organic solvents. *Chem. Mater.* **2017**, *29* (4), 1632−1640.
(39) Mishra, P. C.; Mukherjee, S.; Nayak, S. K.; Panda, A. A brief review on viscosity of nanofluids. *International nano letters* **2014**, *4*, 109−120.
(40) Alqaed, S.; Mustafa, J.; Sharifpur, M.; Cheraghian, G. The effect of graphene nano-powder on the viscosity of water: An experimental study and artificial neural network modeling. *Nanotechnol. Rev.* **2022**, *11* (1), 2768−2785.
(41) Mohammed Zayan, J.; Rasheed, A. K.; John, A.; Khalid, M.; Ismail, A. F.; Aabid, A.; Baig, M. Investigation on rheological properties of water-based novel ternary hybrid nanofluids using experimental and taguchi method. *Materials* **2021**, *15* (1), 28.
(42) Ali, A. R. I.; Salam, B. A review on nanofluid: preparation, stability, thermophysical properties, heat transfer characteristics and application. *SN Appl. Sci.* **2020**, *2* (10), 1636.
(43) Al-Obaidi, M. A.; Rashid, F. L.; Rasheed, M. K.; Aljibori, H. S. S.; Mohammed, H. I.; Mahdi, A. J.; Ahmad, S.; Al-Farhany, K.; Mujtaba, I. M. Recent Achievements in Heat Transfer Enhancement with Hybrid Nanofluid in Heat Exchangers: A Comprehensive Review. *Int. J. Thermophys.* **2024**, *45* (9), 133.
(44) Ma, X.; Song, Y.; Wang, Y.; Yao, S.; Vafai, K. Amelioration of pool boiling thermal performance utilizing graphene-silver hybrid nanofluids. *Powder Technol.* **2022**, *397*, No. 117110.
(45) Sarafraz, M.; Hormozi, F.; Silakhori, M.; Peyghambarzadeh, S. On the fouling formation of functionalized and non-functionalized carbon nanotube nano-fluids under pool boiling condition. *Applied Thermal Engineering* **2016**, *95*, 433−444.
(46) Aydin, E.; El-Demellawi, J. K.; Yarali, E.; Aljamaan, F.; Sansoni, S.; Rehman, A. U.; Harrison, G.; Kang, J.; El Labban, A.; De Bastiani, M.; et al. Scaled Deposition of Ti3C2 T x MXene on Complex Surfaces: Application Assessment as Rear Electrodes for Silicon Heterojunction Solar Cells. *ACS Nano* **2022**, *16* (2), 2419−2428.
(47) Pereira, J.; Moita, A.; Moreira, A. The Pool-Boiling-Induced Deposition of Nanoparticles as the Transient Game Changer—A Review. *Nanomaterials* **2022**, *12* (23), 4270.
(48) Guo, T.; Xu, X.; Liu, C.; Wang, Y.; Lei, Y.; Fang, B.; Shi, L.; Liu, H.; Hota, M. K.; Al-Jawhari, H. A.; et al. Large-area metal−semiconductor heterojunctions realized via MXene-induced two-dimensional surface polarization. *ACS Nano* **2023**, *17* (9), 8324−8332.
(49) Piazza, R. 'Thermal forces': colloids in temperature gradients. *J. Phys.: Condens. Matter* **2004**, *16* (38), S4195.
(50) Braibanti, M.; Vigolo, D.; Piazza, R. Does thermophoretic mobility depend on particle size? *Physical review letters* **2008**, *100* (10), No. 108303.
(51) Das, P. K. A review based on the effect and mechanism of thermal conductivity of normal nanofluids and hybrid nanofluids. *J. Mol. Liq.* **2017**, *240*, 420−446.
(52) Taha-Tijerina, J. J. Thermal transport and challenges on nanofluids performance. *Microfluid. Nanofluid.* **2018**, *1*, 215−256.
(53) Kalpana, G.; Madhura, K.; Kudenatti, R. B. Magneto-hydrodynamic boundary layer flow of hybrid nanofluid with the thermophoresis and Brownian motion in an irregular channel: A numerical approach. *Engineering Science and Technology, an International Journal* **2022**, *32*, 101075.
(54) Kim, S. J.; Bang, I. C.; Buongiorno, J.; Hu, L. Surface wettability change during pool boiling of nanofluids and its effect on critical heat flux. *International journal of heat and mass transfer* **2007**, *50* (19−20), 4105−4116.
(55) Yang, L.; Chen, X.; Xu, M.; Du, K. Roles of surfactants and particle shape in the enhanced thermal conductivity of TiO_2 nanofluids. *AIP Advances* **2016**, *6* (9). DOI: .
(56) Kamatchi, R.; Venkatachalapathy, S.; Nithya, C. Experimental investigation and mechanism of critical heat flux enhancement in pool boiling heat transfer with nanofluids. *Heat and Mass Transfer* **2016**, *52* (11), 2357−2366.
(57) Bahiraei, M. Impact of thermophoresis on nanoparticle distribution in nanofluids. *Results in Physics* **2017**, *7*, 136−138.
(58) Hadžić, A.; Može, M.; Arhar, K.; Zupančič, M.; Golobič, I. Effect of Nanoparticle Size and Concentration on Pool Boiling Heat Transfer with TiO_2 Nanofluids on Laser-Textured Copper Surfaces. *Nanomaterials* **2022**, *12* (15), 2611.
(59) Yao, S.; Teng, Z. Effect of nanofluids on boiling heat transfer performance. *Applied Sciences* **2019**, *9* (14), 2818.
(60) Gobinath, N.; Venugopal, T.; Palani, K.; Samuel, A. A. Numerical modelling of thermophoresis in water-alumina nanofluid under pool boiling conditions. *International Journal of Thermal Sciences* **2018**, *129*, 1−13.
(61) Santos, R.; Moita, A. S.; Ribeiro, A. P. C.; Moreira, A. L. N. The impact of alumina nanofluids on pool boiling performance on biphilic surfaces for cooling applications. *Energies* **2022**, *15* (1), 372.
(62) Sadasivan, P.; Chappidi, P.; Unal, C.; Nelson, R. Possible mechanisms of macrolayer formation. *International communications in heat and mass transfer* **1992**, *19* (6), 801−815.
(63) Liang, G.; Mudawar, I. Review of pool boiling enhancement with additives and nanofluids. *Int. J. Heat Mass Transfer* **2018**, *124*, 423−453.
(64) Wang, H.; Peng, X.; Wang, B.; Lee, D. Bubble-sweeping mechanisms. *Sci. China Ser. E* **2003**, *46* (3), 225−233.
(65) Barber, J.; Brutin, D.; Tadrist, L. A review on boiling heat transfer enhancement with nanofluids. *Nanoscale Res. Lett.* **2011**, *6*, 280.
(66) Ganapathy, H.; Sajith, V. Semi-analytical model for pool boiling of nanofluids. *Int. J. Heat Mass Transfer* **2013**, *57* (1), 32−47.
(67) Ali, N.; Bahman, A. M.; Aljuwayhel, N. F.; Ebrahim, S. A.; Mukherjee, S.; Alsayegh, A. Carbon-based nanofluids and their advances towards heat transfer applications—a review. *Nanomaterials* **2021**, *11* (6), 1628.
(68) Lappan, T. *X-ray and neutron radiography of optically opaque fluid flows: Experiments with particle-laden liquid metals and liquid foams*; Technische Universitat Dresden: 2021.
(69) Gupta, S. K.; Misra, R. D. Experimental pool boiling heat transfer analysis through novel ZnO-coated Cu (Cu@ ZnO nanoparticle) hybrid nanofluid boiling on the fin tops of different microchannels. *J. Therm. Anal. Calorim.* **2023**, *148* (21), 12247−12267.
(70) Gao, T.; Jelle, B. P. Thermal conductivity of TiO_2 nanotubes. *J. Phys. Chem. C* **2013**, *117* (3), 1401−1408.
(71) Slack, G. A. Thermal conductivity of MgO, Al_2O_3, $MgAl_2O_4$, and Fe_3O_4 crystals from 3° to 300° K. *Phys. Rev.* **1962**, *126* (2), 427.

https://doi.org/10.1021/acsomega.4c06988
ACS Omega 2025, 10, 6534−6543

(72) Devi, S. A.; Devi, S. S. U. Numerical investigation of hydromagnetic hybrid Cu−Al_2O_3/water nanofluid flow over a permeable stretching sheet with suction. *Int. J. Nonlin Sci. Num* **2016**, *17* (5), 249−257.
(73) Xie, H.; Yu, W.; Chen, W. MgO nanofluids: higher thermal conductivity and lower viscosity among ethylene glycol-based nanofluids containing oxide nanoparticles. *J. Exp Nanosci* **2010**, *5* (5), 463−472.
(74) Park, S. S.; Kim, N. J. Influence of the oxidation treatment and the average particle diameter of graphene for thermal conductivity enhancement. *Journal of Industrial and Engineering Chemistry* **2014**, *20* (4), 1911−1915.
(75) Xiao, W.; Zhai, X.; Ma, P.; Fan, T.; Li, X. Numerical study on the thermal behavior of graphene nanoplatelets/epoxy composites. *Results in Physics* **2018**, *9*, 673−679.
(76) Eltaweel, M.; Abdel-Rehim, A. A.; Attia, A. A. Energetic and exergetic analysis of a heat pipe evacuated tube solar collector using MWCNT/water nanofluid. *Case Studies in Thermal Engineering* **2020**, *22*, No. 100743.
(77) Gajghate, S. S.; Baratula, S.; Saha, B. B.; Bhaumik, S. Maximizing heat transfer potential with graphene nanofluids along with structured copper surfaces for pool boiling. *Therm. Sci. Eng. Prog.* **2024**, *50*, No. 102559.
(78) Gao, Y.; Hsieh, H.-E.; Zhang, Z.; Wang, S.; Zhou, Z. Experimental study on pool boiling heat transfer characteristics of TiO2 nanofluids on a downward-facing surface. *Prog. Nucl. Energ* **2022**, *153*, No. 104402.
(79) Pare, A.; Ghosh, S. K. Surface qualitative analysis and ANN modelling for pool boiling heat transfer using Al_2O_3-water based nanofluids. *Colloids Surf., A* **2021**, *610*, No. 125926.
(80) Kamel, M. S.; Lezsovits, F. Enhancement of pool boiling heat transfer performance using dilute cerium oxide/water nanofluid: An experimental investigation. *International Communications in Heat and Mass Transfer* **2020**, *114*, No. 104587.
(81) Le Ba, T.; Baqer, A.; Saad Kamel, M.; Gróf, G.; Odhiambo, V. O.; Wongwises, S.; Ferenc, L.; Szilágyi, I. M. Experimental study of halloysite nanofluids in pool boiling heat transfer. *Molecules* **2022**, *27* (3), 729.
(82) Fekadu, B.; Kathiravan, R.; Saravanan, P. Augmentation of pool boiling heat transfer characteristics using naphtha carbon soot nanoparticles−water based nanofluids. *Experimental Heat Transfer* **2022**, *35* (6), 848−863.
(83) Moghadasi, H.; Saffari, H. Experimental study of nucleate pool boiling heat transfer improvement utilizing micro/nanoparticles porous coating on copper surfaces. *International Journal of Mechanical Sciences* **2021**, *196*, No. 106270.
(84) He, K.; Chen, J.; Yu, J.; Liang, L.; Tian, Z. Q. The mechanism of boiling heat transfer of polycarboxylate superplasticizer modified stereotaxically constructed graphene water-based nanofluid: Experiment and molecular dynamics simulation. *Applied Thermal Engineering* **2024**, *246*, No. 122956.
(85) Kamatchi, R. Experimental investigations on nucleate boiling heat transfer of aqua based reduced graphene oxide nanofluids. *Heat and Mass Transfer* **2018**, *54* (2), 437−451.
(86) Moghadam, A. V.; Goshayeshi, H. R.; Chaer, I.; Paurine, A.; Zeinali Heris, S.; Pourpasha, H. Experimental investigation of multiwall carbon nanotubes/water nanofluid pool boiling on smooth and groove surfaces. *International Journal of Energy Research* **2022**, *46* (14), 19882−19893.

https://doi.org/10.1021/acsomega.4c06988
ACS Omega 2025, 10, 6534−6543